Thermopower Modulation Analyses of Effective Channel Thickness for Zn-incorporated In_2O_3-based Thin-Film Transistors

Yuzhang Wu[1], Prashant R. Ghediya[2], Yuqiao Zhang[3], Yasutaka Matsuo[2], Hiromichi Ohta[2,*], and Yusaku Magari[2,*]

[1] *Graduate School of Information Science and Technology, Hokkaido University, N14W9, Sapporo 060-0814, Japan*

[2] *Research Institute for Electronic Science, Hokkaido University, N20W10, Sapporo 001-0020, Japan*

[3] *Institute of Quantum and Sustainable Technology, Jiangsu University, Zhenjiang 212013, China*

*Emails: hiromichi.ohta@es.hokudai.ac.jp, magari.yusaku@es.hokudai.ac.jp

KEYWORDS: Zn-incorporated In_2O_3 TFTs, effective channel thickness, electric field thermopower modulation analysis

ABSTRACT: Zn-incorporated In_2O_3 (IZO) thin-film transistors (TFTs) show high field-effect mobility (μ_{FE} ~40 $cm^2 V^{-1} s^{-1}$) when the IZO channel is amorphous, whereas a lower μ_{FE} (~10 $cm^2 V^{-1} s^{-1}$) is observed with polycrystalline channel. The reasons behind this difference in μ_{FE} remain unclear despite various studies on IZO TFTs. Here, we perform electric field thermopower modulation analysis on amorphous and polycrystalline IZO TFTs to measure the change in effective thickness.

For amorphous channel, the effective thickness was zero when the effective gate voltage ($V_g - V_{th}$, V_g: gate voltage, V_{th}: threshold voltage) was zero. Furthermore, it gradually increased with $V_g - V_{th}$ up to 1.6 nm, reflecting that conduction band bending occurred. By contrast, polycrystalline channel showed an initial effective thickness of 5 nm (≈ film thickness of IZO) and sharply decreased to ~1.7 nm. In amorphous channels, electron transport followed field effect theory, while factors like grain boundaries limited transport in polycrystalline channels.

1. Introduction

Transparent oxide semiconductor (TOS)-based thin-film transistors (TFTs) are widely used as a backplane of present liquid crystal displays and organic light-emitting diode displays, particularly for large-area TV applications. This is because of their higher field-effect mobility (μ_{FE}) of approximately 10 $cm^2 V^{-1} s^{-1}$, which is one or two orders of magnitude higher than that of previously used amorphous Si TFTs (μ_{FE} ~0.5 $cm^2 V^{-1} s^{-1}$)[1-4]. Currently, $InGaZnO_4$-TFTs (μ_{FE} ~10 $cm^2 V^{-1} s^{-1}$)[1-4] are used as the TOS for the display applications. To realize larger area displays with a high definition of 8 K and high-frequency operation of 240 Hz, TOS-based TFTs that exhibit a higher μ_{FE} (> 50 $cm^2 V^{-1} s^{-1}$) are crucial.[5-10]

Among the numerous reports on TOS-TFTs, polycrystalline (large grain size ~several micrometers) In_2O_3-TFTs are considered a promising candidate because of their high μ_{FE} of approximately 100 $cm^2 V^{-1} s^{-1}$.[11, 12] However, In_2O_3-TFTs exhibit poor reliability owing to gas absorption at the In_2O_3 channel surface and grain boundaries.[11] Currently, there are two strategies to address the drawback. The first is using a passivation layer,

and we have previously demonstrated the effectiveness of Y_2O_3 passivation.[13] The second is stabilizing the amorphous phase by incorporating an appropriate concentration of Zn.[14] Although there are homologous phases of $In_2O_3(ZnO)_m$ ($m \geq 3$, integer) in the In-Zn-O system (IZO, hereafter), the crystallization temperature is relatively high (>500 °C) and therefore the amorphous phase is stabilized.

There have been numerous reports on IZO-TFTs[15-28]. Most recently, we reported that the amorphous phase is stabilized when the Zn concentration in the IZO films is between 0.25 and 0.68. In addition, the amorphous IZO-TFTs exhibited a higher μ_{FE} (μ_{FE} ~40 $cm^2\ V^{-1}\ s^{-1}$) than that of polycrystalline IZO-TFTs.[14] However, the origin of the difference in μ_{FE} between amorphous and polycrystalline channels is not sufficiently understood. In this study, we focused on electric-field thermopower modulation analyses of the effective channel thickness of IZO-TFTs with amorphous and polycrystalline channels. Unlike carrier mobility, which reflects the quality of a material (polycrystalline or amorphous) as well as carrier concentration, thermopower solely reflects the volume carrier concentration of a material when the band structure has a simple parabolic shape. By comparing the volume carrier concentration (n_{3D}) dependence of the thermopower (S–n_{3D}) of the bulk material and the sheet carrier concentration (n_{2D}) dependence of S (S–n_{2D}) of the TFT, we can extract the effective channel thickness (t_{eff}) of the TFT; If S of −100 μV K^{-1} is obtained when $n_{3D} = 1 \times 10^{19}$ cm^{-3} and $n_{2D} = 5 \times 10^{12}$ cm^{-3}, then $t_{eff} \equiv n_{2D}/n_{3D}$ is calculated to be 5×10^{-7} cm (= 5 nm). Using the “Electric field thermopower modulation analysis” method, we have clarified the effective channel thickness of $BaSnO_3$-TFTs, SnO_2-TFTs, and AlGaN/GaN HEMTs.[29-34]

In this study, we performed electric field thermopower modulation analysis on amorphous and polycrystalline IZO TFTs to measure the change in effective thickness with gate voltage (V_g) application. In the case of the amorphous IZO channel, the effective thickness was zero when the effective gate voltage ($V_g - V_{th}$, V_{th}: threshold voltage) was zero, and it gradually increased with increasing $V_g - V_{th}$ up to 1.6 nm, reflecting that conduction band bending occurred. By contrast, in the case of the polycrystalline IZO channel, the effective thickness was 5 nm without applying a gate voltage and sharply decreased to approximately 1.7 nm. The electron transport in the amorphous channel is controlled according to the field effect theory, whereas that in the polycrystalline channel is limited by other factors such as grain boundaries.

2. Experimental methods

2.1 Fabrication of IZO-TFTs.[14)] We fabricated IZO-TFTs (bottom-gate and top-contact type) on indium tin oxide (ITO)-coated alkaline-free glass substrates (EAGLE XG®, Corning®). First, a 100-nm-thick amorphous (a-) Al_2O_3 gate insulator was deposited on the substrate by atomic layer deposition. The dielectric permittivity (ε_r) and capacitance (C_i) of the a-Al_2O_3 films were 8 and 70 nF cm^{-2}, respectively. Subsequently, 5-nm-thick IZO films were deposited using pulsed laser deposition (PLD) at room temperature from a ceramic IZO target with various Zn concentrations. The Zn concentrations [atomic ratio presented as Zn/(Zn + In), hereafter] of the resultant IZO films, as measured using inductively coupled plasma mass spectrometry (ICP-MS), were 0.09, 0.25, 0.41, 0.68, and 0.86. The oxygen pressure and laser fluence were maintained at 3 Pa and approximately 1.5 J cm^{-2} pulse^{-1}, respectively. The IZO films were then

annealed in ambient air at 300 °C for 1 h. After annealing, ITO source/drain electrodes were deposited using PLD. Subsequently, a thick Y_2O_3 film of approximately 50 nm was deposited by PLD. This film served as a passivation layer. Finally, the IZO TFTs were annealed at 300 °C in ambient air for 0.5 h. The IZO, ITO, and Y_2O_3 films were deposited using a stencil mask. The channel length (L) and width (W) were 200 μm and 400 μm, respectively. The details of the TFT fabrication are described in a previous study.[14)]

2.2 Structure analyses and electron transport properties measurements of the IZO films

The X-ray diffraction (XRD) patterns of the resulting films were measured using X-ray reflectivity (XRR, ATX-G, Rigaku Co.) (**Supplementary Fig. S1**). The incident angle of the X-rays was fixed at 0.5° while 2θ scanning was performed. The carrier concentration (n), and Hall mobility (μ_{Hall}) of the IZO thin films were measured by a DC four-probe method with a van der Pauw electrode configuration (**Supplementary Fig. S2**). Thermopower (S) was measured using a conventional steady-state method at 25 °C with laboratory-made equipment (**Supplementary Fig. S2**).

2.3 Electric Field Thermopower Modulation Analyses. The transfer characteristics of the IZO TFTs were measured using a semiconductor device analyzer (B1500A, Agilent Technologies) at room temperature in the dark (**Supplementary Table 1**, **Figs. S3** and **S4**). Electric-field thermopower modulation analyses of the IZO TFTs were conducted at room temperature in air, as shown schematically in **Fig. 1**. For the S measurements, two Peltier devices were placed beneath the IZO TFT to create a temperature difference

(ΔT) between the source and drain electrodes. Two thermocouples (K-type, 150 μm in diameter, SHINNETSU Co.) were mechanically attached at both edges of the channel to monitor the temperature difference. The thermoelectromotive force (ΔV) and ΔT values were measured simultaneously at room temperature. The *S*-values were derived from the slope of the ΔV–ΔT plots. Details of the thermopower modulation analyses have been published in previous studies.[29-33)]

3. Results and discussion

We analyzed the effective channel thickness of the IZO TFTs with various Zn concentrations (Zn = 0.09, 0.25, 0.41, 0.68, and 0.86). The Zn concentration of 0.09 and 0.86 were polycrystalline, and those of 0.25, 0.41, and 0.68 were amorphous (**Figure S1**). The amorphous IZO-TFTs exhibited a higher μ_{FE} of approximately 40 $cm^2\ V^{-1}\ s^{-1}$ than that of polycrystalline IZO-TFTs (μ_{FE} ~10 $cm^2\ V^{-1}\ s^{-1}$). The detailed IZO film properties and transistor characteristics of the IZO-TFTs are shown in **Supplementary Table S1** and **Figures S2**, **S3 and S4**. As illustrated in **Fig. 1(a)**, a channel of the IZO TFT was placed in the gap between the two Peltier devices. The ΔT was monitored using two K-type thermocouples (T.C.) located at both edges of the IZO channel. A constant gate voltage (V_g) was then applied to generate a conducting channel. Subsequently, ΔT was introduced using two Peltier devices. Simultaneously, we measured the thermoelectromotive force (ΔV) and ΔT, and calculated the thermopower (*S*) from the slope of $\Delta V/\Delta T$ relationship. As schematically shown in **Fig. 1(b)**, for an n-type channel, if $V_g(1) < V_g(2)$, generally, observable $|S|$ at low $V_g(1)$ is larger than that at high $V_g(2)$.

Figure 2(a) shows typical $\Delta T-\Delta V$ plots for the IZO (Zn = 0.25) TFT upon V_g applications at room temperature. The S values are negative, reflecting that the channel is an n-type semiconductor. When V_g-V_{th} is +10 V, the S is −80 μV K^{-1}, and when V_g-V_{th} is +20 V, S is −56 μV K^{-1}, indicating that the volume carrier concentration (n_{3D}) of the channel increased with increasing V_g. **Figure 2(b)** shows the change in S for the IZO-TFTs as a function of sheet carrier concentration (n_{2D}) that is calculated from $C_i(V_g-V_{th})\cdot e^{-1}$ where C_i is the capacitance per unit area (70 nF cm^{-2} for a-Al_2O_3). Note that the slope of $-S$ vs. log n_{2D} plot for the amorphous channel (Zn = 0.25, 0.41, and 0.68) is milder than that for the polycrystalline channel (Zn = 0.09 and 0.86).

The S values of the IZO films were measured separately (**Figure S5**). We calculated the density of states effective mass (m^*) of the IZO films, except for the Zn concentration of 0.86, and realized that m^* was between 0.1 m_0 and 0.2 m_0. As S reflects the energy derivative of the density of states at the Fermi energy (E_F), the observable S of a semiconductor with a nonparabolic tail state is smaller than that of the parabolic density of states. Therefore, at 0.86 Zn, the tail state near the conduction-band minimum resulted in lower S values.

Then, we extracted the effective channel thickness (n_{2D}/n_{3D}) of the IZO TFTs from the comparison between $-S$ vs. log n_{2D} plot and $-S$ vs. log n_{3D} plot, and plotted them as a function of V_g-V_{th} (**Fig. 3**). The n_{2D}/n_{3D} for the amorphous channels (Zn = 0.25, 0.41, and 0.68) was zero when V_g-V_{th} was zero, and it gradually increased with increasing V_g-V_{th}. In contrast, the n_{2D}/n_{3D} for the polycrystalline channels (Zn = 0.09 and 0.86) was large in the region of a small V_g-V_{th}. As V_g-V_{th} increased, the n_{2D}/n_{3D} converged to

approximately 1.7 nm, a value similar to that of the amorphous channels. These results suggest that the effective channel thickness of the amorphous channel was controlled by the gate voltage, whereas other factors dominated that of the polycrystalline channel.

We discuss the differences between IZO TFTs with amorphous and polycrystalline channels. In the case of the amorphous channel, E_F is located below the conduction band minimum (CBM) when the gate electric field is not applied [**Fig. 4(a)**]. When a positive gate electric field is applied, band bending of the CBM occurs, and a two-dimensional electron gas is formed at the heterointerface between the IZO and a-Al_2O_3 gate insulator. Therefore, the carrier accumulation mechanism of the amorphous channel can be explained by the standard field-effect theory [**Fig. 4(b)**].[35] However, in the case of the polycrystalline channel, a thick conducting channel of approximately 5 nm (≈ film thickness of IZO) is spontaneously formed when the gate electric field is not applied [**Fig. 4(c)**]. This can be attributed to the E_F of polycrystalline IZO located above the CBM. The potential barrier induced by the double Schottky barrier in channel limits mobility when E_F is low, even though V_g = +20 V [**Fig. 4(d)**]. These observations suggest that electron transport in the amorphous IZO channel is controlled according to the standard field-effect theory of nondegenerate semiconductors. In contrast, other factors, such as grain boundaries, limit that in the polycrystalline IZO channel.

4. Conclusions

We performed electric field thermopower modulation analyses on amorphous and polycrystalline IZO TFTs to measure the change in effective thickness with the V_g application. In the case of an amorphous IZO channel, the effective thickness was zero

when the effective gate voltage ($V_g - V_{th}$) was zero. Moreover, the effective thickness gradually increased with increasing $V_g - V_{th}$ up to 1.6 nm, reflecting that conduction band bending occurred. By contrast, in the case of polycrystalline IZO channel, the effective thickness was 5 nm (≈ film thickness of IZO) without gate voltage, and sharply decreased to approximately 1.7 nm with increasing $V_g - V_{th}$. This phenomenon suggests that electron transport in the amorphous channel is controlled according to the normal field effect theory of nondegenerate semiconductors. In contrast, that in the polycrystalline IZO channel is highly limited by other factors, such as potential barriers provided by grain boundaries.

Acknowledgments

Y. Magari was supported by a Grants-in-Aid of the JSPS (22K14303). Y. Zhang was supported by the National Natural Science Foundation of China (Grant No. 52202242), the National Science Foundation of Jiangsu Higher Education Institutions of China (22KJB430002), and the Start-Up Fund of Jiangsu University (5501310015). The authors acknowledge Ms. Nozomi Takeda for the ICP-MS measurements. Part of this study was supported by the Advanced Research Infrastructure for Materials and Nanotechnology in Japan (JPMXP1223HK0082) of the Ministry of Education, Culture, Sports, Science and Technology (MEXT). A part of this work was supported by the Crossover Alliance to Create the Future with People, Intelligence and Materials, and by the Network Joint Research Center for Materials and Devices.

Competing financial interests

The authors declare no competing financial interests.

Associated content

Supporting Information is available free of charge via the Internet at XXXXXXX.

S1. IZO film properties and transistor characteristics of IZO TFTs. Field effect mobility (μ_{FE}), threshold voltage (V_{th}), and subthreshold swing of the IZO TFTs with varied Zn concentration; Table S1. Grazing incident XRD patterns of the resultant IZO films; Figure S1. Electron transport properties of the IZO films at room temperature; Figure S2. Typical transfer characteristics of IZO TFTs at room temperature; Figure S3. Output characteristics of the IZO TFTs with Zn = 0.25; Figure S4. Changes in thermopower as a function of carrier concentration in the IZO films; Figure S5. Thermopower of the IZO films with various Zn concentrations.

Author information

Corresponding Authors

Hiromichi Ohta – Research Institute for Electronic Science, Hokkaido University, N20W10, Kita, Sapporo 001-0020, Japan

ORCID: orcid.org/0000-0001-7013-0343

Email: hiromichi.ohta@es.hokudai.ac.jp

Yusaku Magari – Research Institute for Electronic Science, Hokkaido University, N20W10, Kita, Sapporo 001-0020, Japan

ORCID: orcid.org/0000-0001-9655-4283

Email: magari.yusaku@es.hokudai.ac.jp

Author

Yuzhang Wu – Graduate School of Information Science and Technology, Hokkaido University. N14W9, Kita Sapporo 060-0814, Japan

ORCID: orcid.org/0000-0002-6173-4994

Prashant R. Ghediya – Research Institute for Electronic Science, Hokkaido University, N20W10, Kita, Sapporo 001-0020, Japan

ORCID: orcid.org/0000-0001-9953-0471

Yuqiao Zhang – Institute of Quantum and Sustainable Technology, Jiangsu University, Zhenjiang 212013, China

ORCID: orcid.org/0000-0001-7579-4923

Yasutaka Matsuo – Research Institute for Electronic Science, Hokkaido University, N20W10, Kita, Sapporo 001-0020, Japan

ORCiD: orcid.org/0000-0002-5071-0284

Author Contributions

Y. W. and P. R. G. fabricated the samples and measured the transistor characteristics and thermopower properties. Y. Z. analyzed the thermopower. Y. Matsuo fabricated a-Al_2O_3 gate insulator films. H. O. and Y. Magari planned and supervised the project. All the authors discussed the results and commented on the manuscript.

Funding

Yusaku Magari received funding from Grants-in-Aid of the JSPS (22K14303). Yuqiao Zhang was supported by the National Natural Science Foundation of China (Grant No. 52202242), the National Science Foundation of Jiangsu Higher Education Institutions of China (22KJB430002), and the Start-Up Fund of Jiangsu University (5501310015).

Notes

The authors declare no competing interest.

References

1) K. Nomura, H. Ohta, A. Takagi, T. Kamiya, M. Hirano and H. Hosono, Nature. **432**, 488 (2004).

2) T. Kamiya and H. Hosono, NPG Asia Materials. **2**, 15 (2010).

3) E. Fortunato, P. Barquinha and R. Martins, Adv. Mater. **24**, 2945 (2012).

4) H. Hosono, Nat. Electron. **1**, 428 (2018).

5) J.Y. Kwon and J.K. Jeong, Semicond Sci Tech. **30**, 024002 (2015).

6) Y. Hara, T. Kikuchi, H. Kitagawa, J. Morinaga, H. Ohgami, H. Imai, T. Daitoh and T. Matsuo, J. Soc. Inf. Display. **26**, 169 (2018).

7) H. I., B. J. and M. S., Inf. Display. **38**, 60 (2022).

8) T. Kim, C.H. Choi, J.S. Hur, D. Ha, B.J. Kuh, Y. Kim, M.H. Cho, S. Kim and J.K. Jeong, Adv. Mater. **35**, e2204663 (2023).

9) M.J. Kim, H.J. Park, S. Yoo, M.H. Cho and J.K. Jeong, IEEE Trans. Electron Dev. **69**, 2409 (2022).

10) F. Mo, T. Saraya, T. Hiramoto and M. Kobayashi, Appl. Phys. Express. **13**, 074005 (2020).

11) Y. Magari, T. Kataoka, W. Yeh and M. Furuta, Nat. Commun. **13**, 1078 (2022).

12) J.K. Jeong, H. Won Yang, J.H. Jeong, Y.-G. Mo and H.D. Kim, Appl. Phys. Lett. **93**, 123508 (2008).

13) P.R. Ghediya, Y. Magari, H. Sadahira, T. Endo, M. Furuta, Y. Zhang, Y. Matsuo and H. Ohta, Small Methods, 2400578 (2024).

14) Y. Wu, Y. Magari, P.R. Ghediya, Y. Zhang, Y. Matsuo and H. Ohta, Jpn. J. Appl. Phys. **63**, 076504 (2024).

15) J.C. Park, H.N. Lee and S. Im, ACS Appl. Mater. Interfaces. **5**, 6990 (2013).

16) H. Ji, A.Y. Hwang, C.K. Lee, P.S. Yun, J.U. Bae, K.S. Park and J.K. Jeong, IEEE Trans. Electron Dev. **62**, 1195 (2015).

17) Z. Yang, J.W. Yang, T. Meng, M.Y. Qu and Q. Zhang, Mater. Lett. **166**, 46 (2016).

18) J.W. Zhao, X.A. Zhang, S. Li, H.W. Zheng, G. Yang and W.F. Zhang, Phys. Stat. Sol. A. **214**, 1600315 (2016).

19) A. Illiberi, I. Katsouras, S. Gazibegovic, B. Cobb, E. Nekovic, W. van Boekel, C. Frijters, J. Maas, F. Roozeboom, Y. Creyghton, P. Poodt and G. Gelinck, J. Vac. Sci. Technol. A. **36**, 04F401 (2018).

20) J.M. Lee, H.J. Lee, J.E. Pi, J.H. Yang, J.H. Lee, S.D. Ahn, S.Y. Kang and J. Moon, J. Vac. Sci. Technol. A. **37**, 060910 (2019).

21) J. Sheng, T. Hong, D. Kang, Y. Yi, J.H. Lim and J.S. Park, ACS Appl. Mater. Interfaces. **11**, 12683 (2019).

22) M.Y. Liu, H. Kim, X.Y. Wang, H.W. Song, K. No and S. Lee, ACS Appl. Electron. Mater. **3**, 2703 (2021).

23) M.H. Cho, C.H. Choi and J.K. Jeong, ACS Appl. Mater. Interfaces. **14**, 18646 (2022).

24) E. Fortunato, P. Barquinha, A. Pimentel, L. Pereira, G. Gonçalves and R. Martins, Phys. Stat. Sol. (RRL) **1**, R34 (2007).

25) E. Fortunato, P. Barquinha, G. Goncalves, L. Pereira and R. Martins, Solid State Electron. **52**, 443 (2008).

26) J. Sheng, H.J. Lee, S. Oh and J.S. Park, ACS Appl. Mater. Interfaces. **8**, 33821 (2016).

27) Y.K. Liang, J.W. Lin, L.C. Peng, Y.M. Hua, T.T. Chou, C.C. Kei, C.C. Lu, H.Y. Huang, S.H. Yeong, Y.M. Lin, P.T. Liu, E.Y. Chang and C.H. Lin, IEEE Trans. Electron Dev. **70**, 1067 (2023).

28) S. Jeon, S.D. Ahn, I. Song, C.J. Kim, U.I. Chung, E. Lee, I. Yoo, A. Nathan, S. Lee, K. Ghaffarzadeh, J. Robertson and K. Kim, Nat. Mater. **11**, 301 (2012).

29) A.V. Sanchela, T. Onozato, B. Feng, Y. Ikuhara and H. Ohta, Phys. Rev. Mater. **1**, 034603 (2017).

30) H. Ohta, S.W. Kim, S. Kaneki, A. Yamamoto and T. Hashizume, Adv. Sci. **5**, 1700696 (2018).

31) A.V. Sanchela, M. Wei, H.J. Cho and H. Ohta, Small **15**, 1805394 (2019).

32) D.D. Liang, Y.Q. Zhang, H.J. Cho and H. Ohta, Appl. Phys. Lett. **116**, 143503 (2020).

33) H. Yang, Y.Q. Zhang, Y. Matsuo, Y. Magari and H. Ohta, ACS Appl. Electron. Mater. **4**, 5081 (2022).

34) P. Ghediya, H. Yang, T. Fujimoto, Y.Q. Zhang, Y. Matsuo, Y. Magari and H. Ohta, J. Phys. Chem. C. **127**, 2022 (2023).

35) S.M. Sze, Y. Li and K.K. Ng, *Physics of semiconductor devices* (John wiley & sons, 2006).

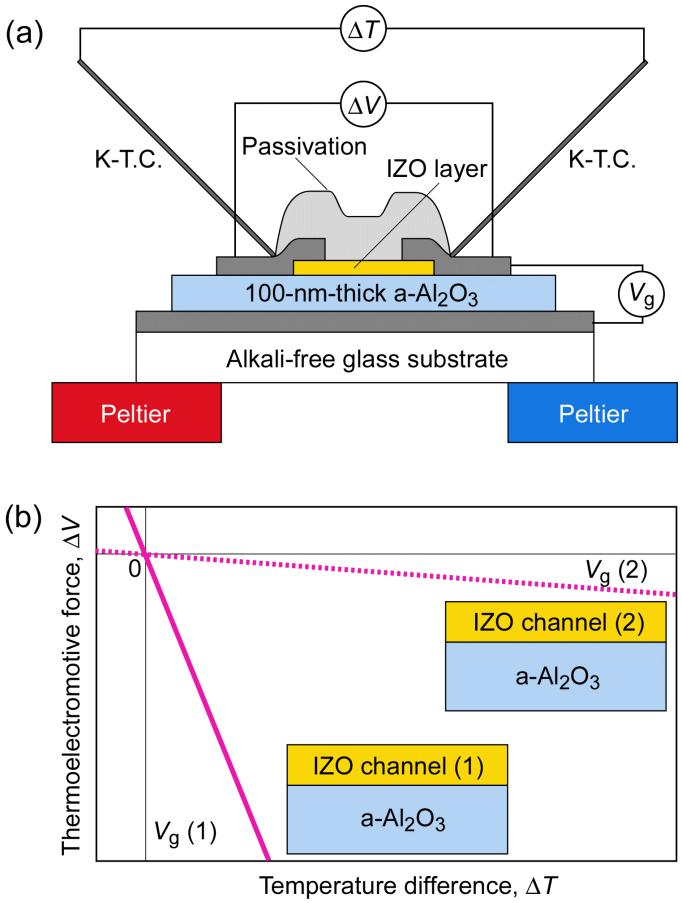

Figure 1. Schematic electric-field thermopower modulation method of the In-Zn-O TFTs. (a) Schematic illustration of the measurement setup. Bottom-gate top-contact TFTs were fabricated using 5-nm-thick In-Zn-O channel layers on alkali-free glass substrates. The channel length (L) is 200 μm and the channel width (W) is 400 μm. A 100-nm-thick amorphous (a-) Al_2O_3 ($\varepsilon_r = 8$, $C_i = 70$ nF cm^{-2}) was used as the gate insulator. ITO films were used as the source, drain, and gate electrodes. The In-Zn-O channel surface was passivated using a polycrystalline Y_2O_3 layer to stabilize the electron transport properties of the In-Zn-O layer when gating. The channel was placed on the gap between two Peltier devices, one hot and the other cold, to introduce a temperature difference (ΔT). The ΔT was monitored using two K-type thermocouples (T.C.) located at both edges of the In-Zn-O channel. The thermoelectromotive force (ΔV) was measured when ΔT was introduced to the channel. (b) Schematic relationship between ΔT and ΔV of a TFT based on n-type semiconductor like In-Zn-O channel. From the slope of the $\Delta V/\Delta T$ relationship, the thermopower (S) can be calculated. For an n-type channel, if $V_g(1) < V_g(2)$, generally, observable $|S|$ at low $V_g(1)$ is larger than that at high $V_g(2)$.

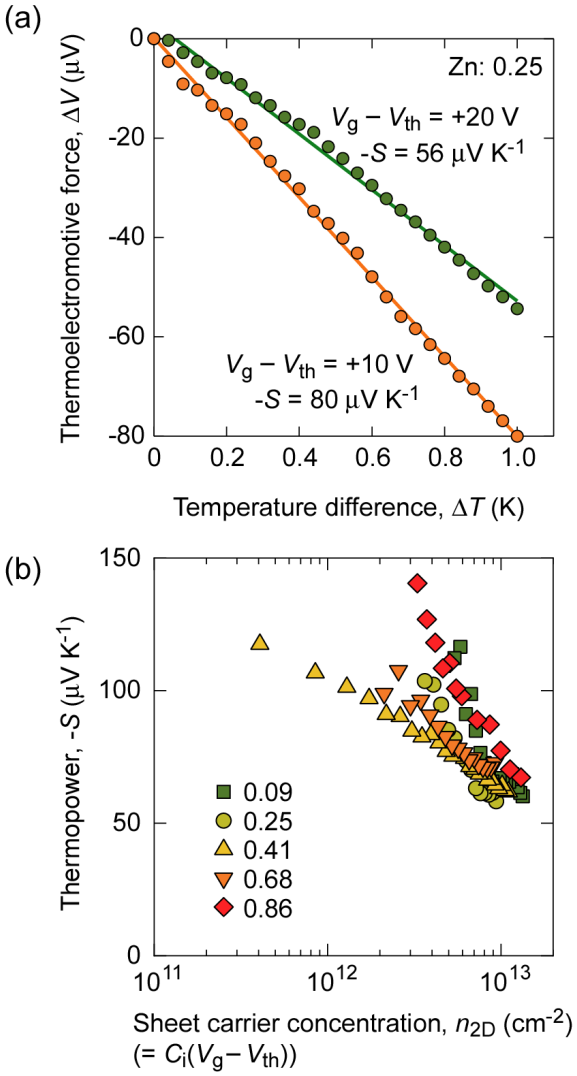

Figure 2. **Thermopower of the IZO-TFTs.** (a) ΔT–ΔV plots for the IZO (Zn = 0.25) -TFT upon V_g applications at room temperature. The S values are negative, reflecting the channel is an n-type semiconductor. When V_g–V_{th} is +10 V, S is −80 μV K^{-1}, and when V_g–V_{th} is +20 V, S is −56 μV K^{-1}, indicating that the volume carrier concentration of the channel increases with increasing V_g. (b) Change in S for the IZO-TFTs as a function of sheet carrier concentration (n_{2D}) that is calculated from $C_i(V_g - V_{th})$. Note that the slope of −S vs. log n_{2D} plot for the amorphous channel (Zn = 0.25, 0.41, and 0.68) is milder than that for the polycrystalline channel (Zn = 0.09 and 0.86).

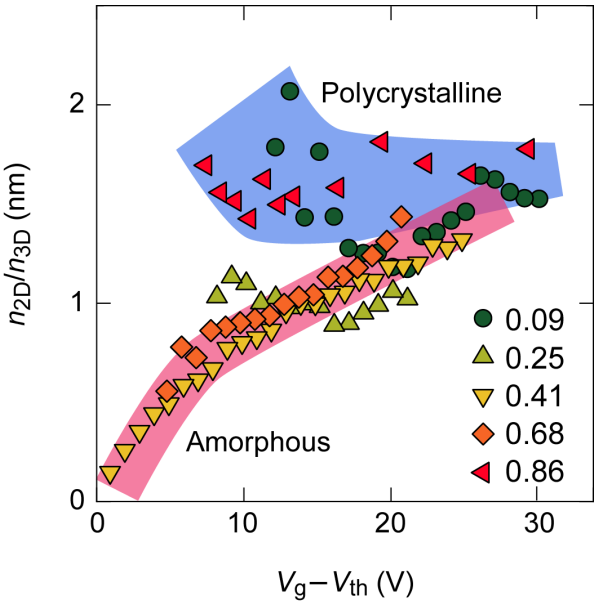

Figure 3. **Change in the effective channel thickness (n_{2D}/n_{3D}) of the IZO-TFTs as a function of $V_g - V_{th}$.** The n_{2D}/n_{3D} for the amorphous channels (Zn = 0.25, 0.41, and 0.68) is zero when $V_g - V_{th}$ is zero and gradually increases with increasing $V_g - V_{th}$. In contrast, the n_{2D}/n_{3D} for the polycrystalline channels (Zn = 0.09 and 0.86) is large in the region of a small $V_g - V_{th}$. As $V_g - V_{th}$ increases, the n_{2D}/n_{3D} converges to approximately 1.7 nm, a value similar to that of the amorphous channels.

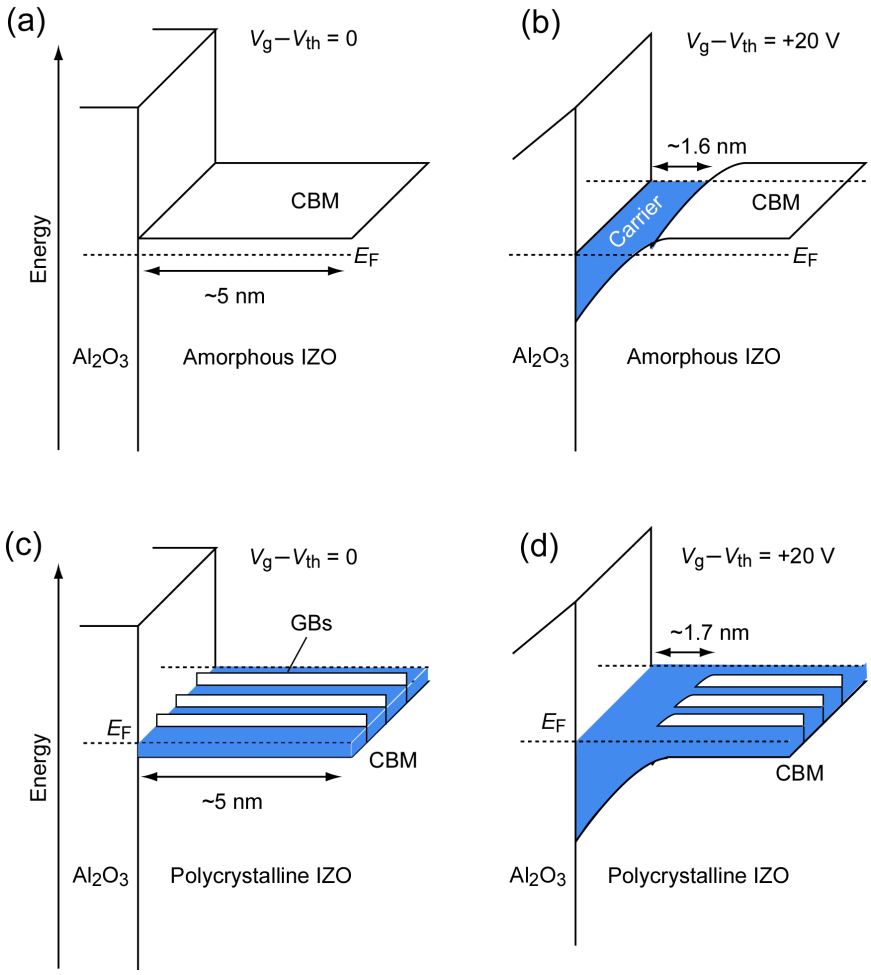

Figure 4. Schematic operation mechanism of the IZO-TFTs with amorphous channel and polycrystalline channel. In the case of the amorphous channel, (a) the E_F locates below the conduction band minimum (CBM) when the gate electric field is not applied ($V_g - V_{th}$). (b) When a positive gate electric field is applied, band bending of the CBM occurs, and a two-dimensional electron gas is formed at the heterointerface between IZO and Al_2O_3. Thus, the carrier accumulation mechanism of the amorphous channel is explained as the standard field effect theory. In the case of the polycrystalline channel, (c) a thick conducting channel of approximately 5 nm (≈ film thickness of IZO) is spontaneously formed when the gate electric field is not applied. Thus, the E_F locates above the CBM, and (d) gate electric field application might enhance the mobility. Since there are many grain boundaries in the channel, potential barriers, i.e., double Schottky barrier, limit mobility when the E_F is low.